applied sciences

MDPI

Article

Effect of Platinum Doping on the Morphology and Sensing Performance for CuO-Based Gas Sensor

Qi Tang [1,2,†], Xiao-Bing Hu [2,†], Meng He [2], Li-Li Xie [2], Zhi-Gang Zhu [2,*] and Jian-Qing Wu [1,*]

1 School of Materials Science and Engineering, South China University of Technology, Guangzhou 510641, China; 13702752760@139.com

2 School of Environmental and Materials Engineering, College of Engineering, Shanghai Polytechnic University, Shanghai 201209, China; xiaobinghu1992@foxmail.com (X.-B.H.); menghesspu@163.com (M.H.); llxie@sspu.edu.cn (L.-L.X.)

* Correspondence: zgzhu@sspu.edu.cn (Z.-G.Z.); imjqwu@scut.edu.cn (J.-Q.W.); Tel.: +86-21-5021-1236 (Z.-G.Z.)

† These authors contributed equally to this work.

Received: 21 May 2018; Accepted: 28 June 2018; Published: 5 July 2018

Featured Application: This gas sensor can be used for air quality monitoring, food processing and the detection of toxic, flammable and explosive gases.

Abstract: Pristine and Pt-doped CuO nano-flowers were synthesized by a simple water bath heating method in this paper. Highly sensitive hydrogen sulfide (H_2S) gas sensors based on Pt-doped CuO nano-flowers were fabricated. Scanning electron microscopy, X-ray diffraction, inductively coupled plasma atomic emission spectrometry, and energy dispersive X-ray spectroscopy were used to examine the characteristics and morphology of materials. The sensing performances of sensors with different concentrations of Pt dopants were evaluated at different operating temperatures. The results indicated that the CuO sensor doped with 1.25 wt % Pt exhibited the highest response (R_g/R_a, where R_g is the resistance in gas, and R_a is the resistance in air) of 135.1 to 10 ppm H_2S at 40 °C, which was 13.1 times higher than the response of a pure CuO sensor. Pt doping also plays an important role for the enhancement of H_2S selectivity against C_2H_5OH, NH_3, H_2, CH_3COCH_3, and NO_2.

Keywords: CuO; gas sensor; Pt doping; low temperature

1. Introduction

Hydrogen sulfide (H_2S) is a toxic, harmful, and malodorous gas, which is usually produced by petroleum refining, as well as agricultural and biogas production [1–3]. The threshold limit value for H_2S gas (recommended by the American Conference of Government Industrial Hygienists) is 10 ppm [4]. Furthermore, H_2S gas is liable to explode at a high temperature. Therefore, it is urgent to develop a new type of sensors for detecting H_2S with a low operating temperature. Although researchers have developed some detecting methods, such as fluorescent probes [5], electrogenerated chemiluminescene [6], and chemical methods [7] to detect H_2S, these methods still have shortcomings such as complex detection process, and high cost. Among the various detection methods, metal oxide semiconductor gas sensors have been widely used in the detecting of toxic, flammable, and explosive gases; monitoring air quality; and food processing, due to their simplicity, high sensitivity, low cost, and compatibility with modern electronic devices [8,9]. In recent years, many researchers have utilized metal oxide semiconductor sensors to detect H_2S gas, including CuO [10,11], In_2O_3 [12], ZnO [13,14] SnO_2 [15], and WO_3 [16]. Cupric oxide (CuO), as a typical

p-type semiconductor with a band gap of 1.2 eV [17], has been widely investigated in lithium-ion batteries [18], super-capacitors [19], heterogeneous catalysts [20], and particularly in gas detection devices. The gas sensitivity of CuO-based gas sensors has been widely reported. Ramgir et al. [10] reported H_2S gas sensors based on CuO thin films, and the results showed that the response of CuO thin films to sub-ppm (100–400 ppb) H_2S at room temperature was highly reversible. However, once the concentration was higher than 400 ppb, the response became irreversible. To improve the performance of sensors, loading metal oxides with catalytic metals or noble metals nanoparticles on the surface has proved to be a very effective method [21]. For example, Kang et al. [22] reported that 2.2 wt % Cr added to CuO nanostructures by a solvothermal reaction significantly increased the responses to 100 ppm NO_2 from 7.5 to 134.2. Kim et al. [23] prepared Pd functionalized one-dimensional CuO nanostructures, which revealed a high response of 167 at 50 ppm. However, the operating temperature was relatively high (300 °C). Therefore, there is still a great demand to develop a H_2S gas sensor with excellent sensing performance, such as fast response/recovery time, good selectivity, high sensitivity, low detection limit, and relatively low operating temperature [24].

Pt as a catalytic additive has been proven to be effective in improving gas-sensing performance. Ivanov et al. [25] has shown that the Pt-doped SnO_2 material is less resistant, more sensitive, and shows faster response to ethanol than pure SnO_2; what's more, the response of the Pt-doped sensors was between 2 and 55 times higher than the commercial one. Wang et al. [26] prepared α-Fe_2O_3 nanoparticles doped with different amounts of Pt. Compared with the pure α-Fe_2O_3 based sensor, the Pt-doped α-Fe_2O_3 based sensors showed the enhanced excellent sensing performance and good selectivity for H_2S gas. However, reports on the gas-sensing performance of Pt-doped CuO are rather rare. We expected that Pt doping could be an efficient way to enhance the sensing properties of pure CuO. In the present work, the pristine and Pt-doped CuO based H_2S gas sensors were designed. The Pt-doped CuO has been prepared using a facile one step method. For the purpose of comparison, the gas sensing performance of CuO sensors with different Pt concentrations was evaluated. The effect of Pt doping plays an important role in enhancing the sensing performance, and the resulting gas sensors are able to operate at a low temperature. Long recovery time is a common issue for the metal oxide semiconductor sensors at low operating temperature [27], and we found that applying a short electric current pulse is an appropriate way to reduce the recovery time.

2. Experimental

All chemicals used in this work were of analytical grade and were used without further purification, and were purchased from Sinopharm Chemical Reagent Co. Ltd. (Shanghai, China).

2.1. Preparation of CuO

CuO nanoflowers were synthesized by a simple water bath heating method. The typical process is listed here: 24.16 g copper (II) nitrate hydrate was dissolved in 1000 mL deionized water to prepare copper nitrate solution (0.1 mol/L), and then 12.62 g hexamethylenetra-mine was then added into the above solution (20 mL), and stirred for 1 h to get a bright blue solution. After that, the flask was moved to a water bath container at 80 °C for 90 min, and the bright blue Cu-hydroxide precipitate converted into dark brown ones (copper oxide). Finally, the resulting mixture was allowed to cool to room temperature, and was subsequently subjected to centrifugation at 8000 rpm for 10 min. The samples were rinsed with deionized water three times, followed by three times with ethanol, and were dried in the oven at 80 °C.

2.2. Pt-Doped CuO Flowers

Pt-doped CuO flowers were prepared by the following procedure: Chloroplatinic acid hexahydrate (1 g) was dissolved in deionized water (100 mL) to prepare mother liquor, then, the above solution (12.95 mL) was diluted to 250 mL to prepare (hydro)chloroplatinic acid (1 mmol/L). After that, a copper nitrate solution (20 mL) and (hydro)chloroplatinic acid were mixed together, and the

remaining steps were the same as mentioned above. For a convenient comparison, we indicate doping with different concentrations of Pt by 0.75Pt-CuO, 1.25Pt-CuO, and 1.50Pt-CuO, respectively, which means the Pt doping concentration in the copper nitrate solution were 0.75 wt %, 1.25 wt %, and 1.50 wt %, respectively.

2.3. Characterization

The crystallinity and phase composition of the CuO specimens were analyzed by X-ray diffraction with a monochromatized Cu target radiation resource (λ = 1.5418 Å), scanning from 10–80° (XRD, D8-Advance, Bruker, Germany), as well as X-ray photoelectron spectroscopy (XPS, ESCALAB 250Xi, Thermo Scientific, London, UK). The morphology of the powders was investigated by field emission scanning electron microscopy (FE-SEM, S-4800, Hitachi Co. Ltd., Tokyo, Japan) at an accelerating voltage of 10 kV. Energy Dispersive X-Ray (EDX) spectroscopy was used to confirm the composition of the CuO nanostructures. The surface areas were measured by the Brunauer–Emmett–Teller method (BET, Tristar II 3020, Micromeritics Instrument Co Ltd., Norcross, GA, USA). The concentrations of Pt-doped specimens were determined by inductively coupled plasma atomic emission spectrometer (ICP-AES, A-6300, Thermo Scientific, Waltham, MA, USA).

2.4. Fabrication and Characterization of Gas Sensors

Gas sensors based on bare CuO and Pt-doped CuO products were fabricated. The gas sensors were fabricated as follows: The as-synthesized Pt-doped CuO flowers were uniformly mixed with deionized water to prepare a paste, and were then coated onto a ceramic tube with a pair of gold electrodes at both ends to form a thick film. The ceramic tubes were heated and dried under infrared radiant heating. Figure 1a shows a schematic structure of the ceramic electrode. The sensing element was calcined at 500 °C for 2 h to remove the bound water and to form a porous structure on the surface for gas sensing. After cooling down, a heating wire was placed inside the ceramic tube to make sure the sensors can work at different operating temperatures. Finally, the sensors were aged at 5.0 V for 7 days, in order to stabilize it. The photograph of the gas sensor is shown in Figure 1b.

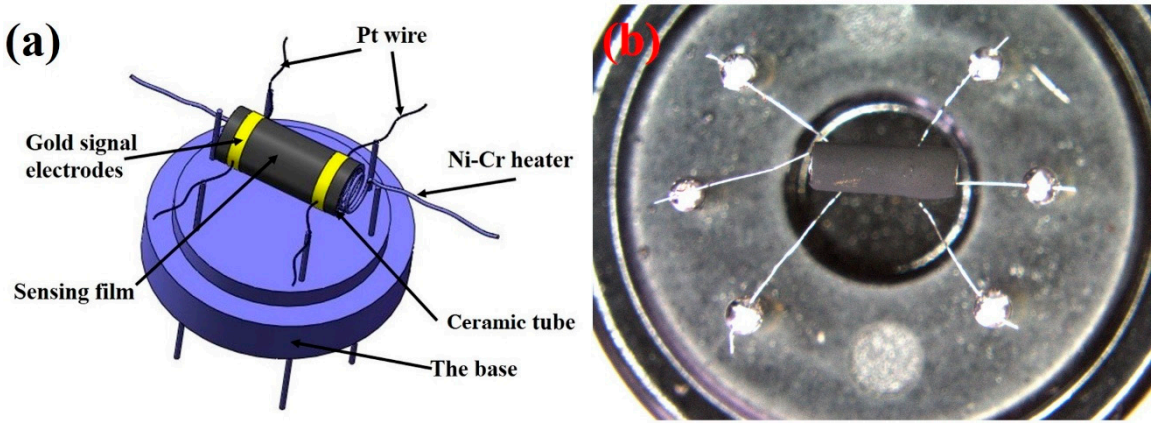

Figure 1. (**a**) Schematic illustration of the gas sensor and (**b**) photographs of the gas sensor.

The WS-30A Gas Sensing Analysis System (Weisheng Tech Co, Ltd., Zhengzhou, China) was used to measure the performance of the gas sensor, and the static testing method was applied to examine the gas sensing performance. The gas sensors were placed into a closed test chamber (15 L in volume), and the target gases were injected into the test chamber through a rubber plug. The electrical properties changed once the sensor was exposed to the target gas. When the response reached a constant value, the sensors were exposed to air again, and the response returned to its original value. The response was defined as the ratio of R_a to R_g or R_g to R_a, where R_a and R_g are the resistances in the air and

target gas, respectively. The response and recovery time were defined as the time needed for the sensor to reach 90% of the total change of the resistance during adsorption and desorption, respectively.

3. Results and Discussions

3.1. Structure and Morphology of Sensing Materials

Figure 2 plots the XRD patterns of pure CuO structures and Pt-doped CuO structures. The patterns of pure CuO are specified as monoclinic CuO (JCPDS No. 72-0629), and reveal a series of well-defined diffraction peaks at 2θ of 32.53°, 35.56°, 38.75°, 48.75°, 53.50°, 58.36°, 61.57°, 66.28°, and 67.97°, corresponding to the (110), (−111), (111), (−202), (020), (202), (−113), (−311), and (113) planes of monoclinic CuO. All XRD patterns look very similar at first sight, as shown in Figure 2a. However, the difference can be found at the specific region (35–40°) of XRD patterns in Figure 2b. After Cu^{2+} ions had been replaced by Pt^{2+} ions in the CuO matrix, the lattice parameter of CuO crystal is changed because of the different ionic radius between Cu^{2+} (0.73 Å) [28] and Pt^{2+} (0.86 Å) [29]. As a result, with the increase of the Pt dopant from 0.75 wt % to 1.50 wt %, the (−111) and (111) peaks were slightly shifted to a lower angle [30]. What is more, we used the least square refinement method in the unit cell program to determine the lattice constants. The obtained parameters of the 1.25 wt % Pt-doped CuO are α = 4.6837 Å, b = 3.4226 Å, and c = 5.1288 Å, and the unit cell volume is 82.2169 $Å^3$. The lattice constants of the doped sample are the monoclinic data of undoped CuO (α = 4.6504 Å, b = 3.3903 Å, c = 5.0997 Å, and unit cell volume = 80.4032 $Å^3$) obtained under the same conditions. It can be seen that the unit cell expands with the Pt^{2+} ion doping in CuO. This clearly proved that the Pt^{2+} ions were successfully replaced by Cu^{2+} in the CuO matrix.

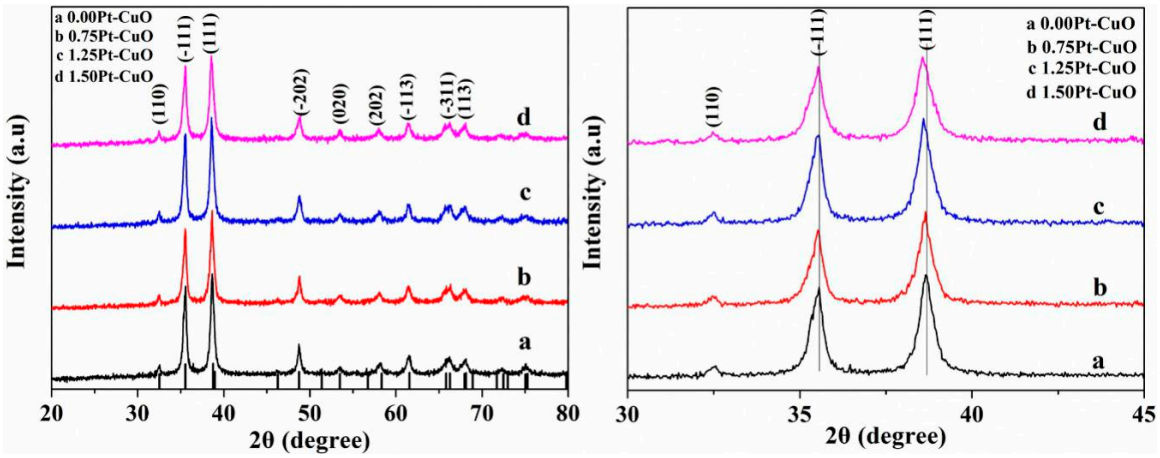

Figure 2. X-ray diffraction (XRD) pattern of the Pt-doped CuO specimens: (**a**) 0.00Pt-CuO, (**b**) 0.75Pt-CuO, (**c**) 1.25Pt-CuO, and (**d**) 1.50Pt-CuO.

Field emission scanning electron microscope (FESEM) images of pristine CuO and Pt-doped CuO with various doping concentrations are shown in the Figure 3. As shown in Figure 3a, the morphology of the pristine CuO was olive-like, exhibiting particle diameters ranging from 200 nm to 4 μm. Once the Pt^{2+} ions were introduced, the morphology of the CuO structure transformed into being flower-like, as illustrated in Figure 3b,c. At a Pt doping concentration of 1.25 wt % (Figure 3c), a three-dimensional (3D) flower-like CuO with hierarchical nanostructures was obtained. The flower-like CuO is ca. 1.5 μm in diameter and homogeneously distributed, and the hierarchical flower-like CuO consists of nanosheets with sizes around 200 nm. The resulting growth-mechanism for CuO after Pt doping can be explained as follows: A copper nitrate solution provides Cu^{2+} ions to form a blue precipitate of copper hydroxide $Cu(OH)_2$. The color of the $Cu(OH)_2$ precipitate gradually turned into dark brown, which was caused by the dehydration of $Cu(OH)_2$ and finally formed the nano-CuO along with the

increase of the water bath temperature. Once the Pt was introduced, it did not affect the precipitate color, but seemed to have a consecutive influence on the growth rate of the nanoflower CuO [31]. The Pt ions tend to be adsorbed on the basal planes of the CuO, and hence modify the chemical surface properties of CuO, such as the relative surface free energy on the facets. It was also observed that the presence of higher amounts of Pt influenced the dehydration of $Cu(OH)_2$ and retarded the phase transformation of the $Cu(OH)_2$ to CuO. In addition, the morpholoies of the CuO were not significantly altered after increasing the Pt doping concentration to 1.50 wt %, instead, the uniformity of the CuO declined again (Figure 3d). Thus, it was clearly demonstrated that the morphology of CuO can be adjusted by the Pt doping.

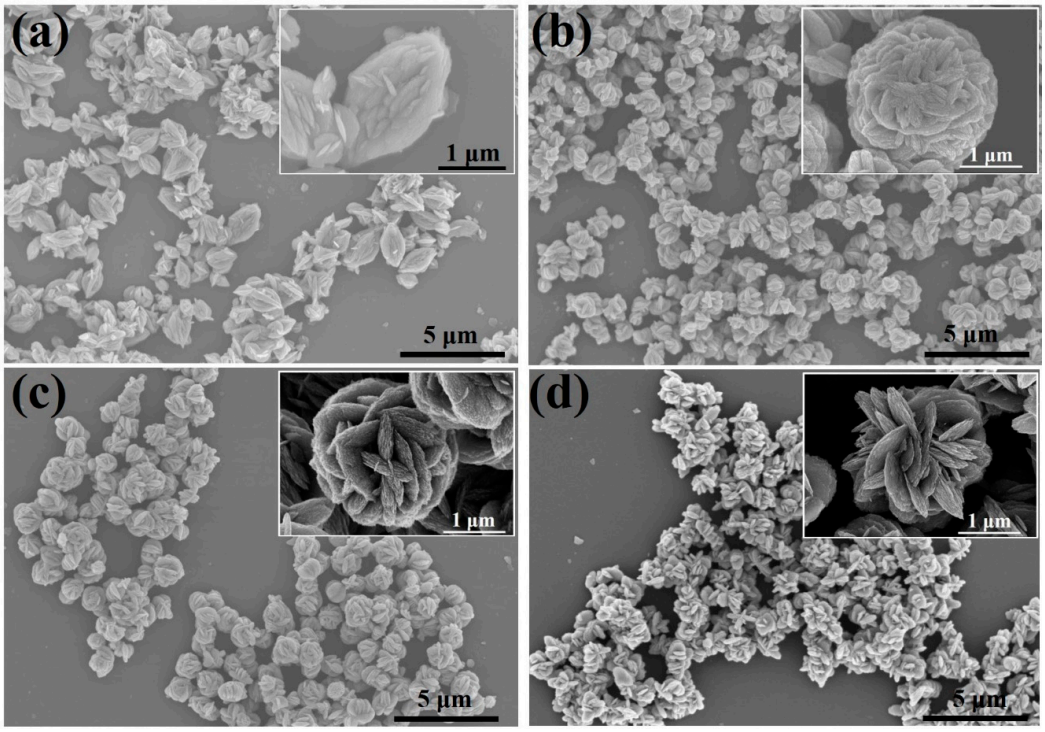

Figure 3. Field emission scanning electron microscope (FESEM)images of (**a**) 0.00Pt-CuO, (**b**) 0.75Pt-CuO, (**c**) 1.25Pt-CuO, and (**d**) 1.50Pt-CuO. The inset is the magnification of each image.

The EDX element mapping was employed to evaluate the uniformity of element distribution in a 1.25Pt-CuO specimen. Figure 4 shows the distribution of the O, Cu, and Pt, respectively, and it is clearly demonstrated that all three elements are homogeneously distributed. Meanwhile, the concentrations of the 1.00Pt-CuO, 1.25Pt-CuO, and 1.50Pt-CuO specimens were also determined by inductively coupled plasma mass spectroscopy, the Pt concentrations were 0.76 at%, 0.85 at%, and 0.91 at%, respectively.

The XPS spectral measurements were used to analyze the chemical states of the 1.25Pt-CuO sample. The full spectra of 1.25Pt-CuO are shown in Figure 5a, which proved the existence of Cu, Pt, and O. The appearance of the C 1s peaks can be ascribed to the adsorbed or bonded organic species [32]. In Figure 5b, two peaks at 933.4 eV and 953.2 eV, corresponding to Cu $2p_{3/2}$ and Cu $2p_{1/2}$, denote the existence of Cu^{2+} in the form of CuO. In addition, the satellite peaks of Cu $2p_{3/2}$ and Cu $2p_{1/2}$, denoted as peaks S1 and S2, respectively, are characteristic for a partially filled d-orbital (3 d_9 in the case of Cu^{2+}) [33]. The Pt 4f spectra of 1.25Pt-CuO are shown in Figure 5c. After the Pt 4f curve fitting (Figure 5c), the spectrum consists of two pairs of peaks at 74.7 and 76.5 eV and at 75.6 and 77.9 eV, which are assigned to Pt^0 and Pt^{2+}, respectively [34]. The above measurements clearly proved that the Pt^{2+} ions were successfully doped into the CuO matrix, which is in good accordance with the results of EDX and ICP-AES. Figure 5d shows the high-resolution O 1s XPS profile of Pt-doped CuO, in which the two peaks at binding energies of 529.4 eV and 531.1 eV correspond to the typical surface

lattice oxygen and the surface absorbed oxygen species ($O_2^-{}_{ads}$ and $O^-{}_{ads}$) [35]. The surface absorbed oxygen species play a positive role in the enhancement of gas sensing performance, as they are capable of reacting with test gas molecules [36].

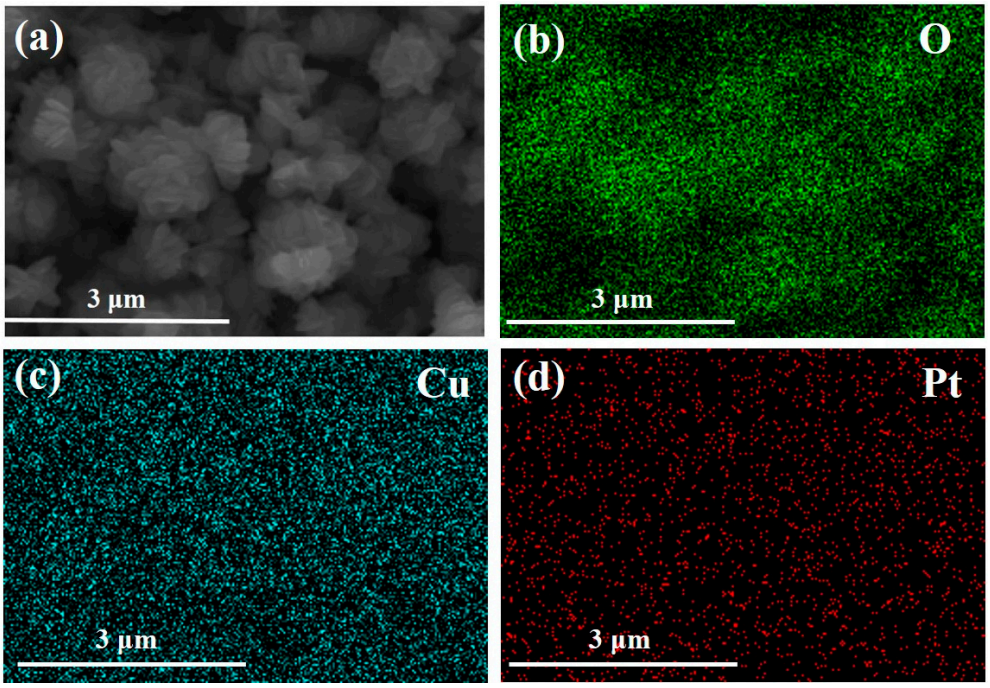

Figure 4. Energy Dispersive X-Ray (EDX) element mapping of 1.25 wt % Pt-doped CuO structure, as follows: (**a**) 1.25Pt-CuO, (**b**) O, (**c**) Cu, and (**d**) Pt.

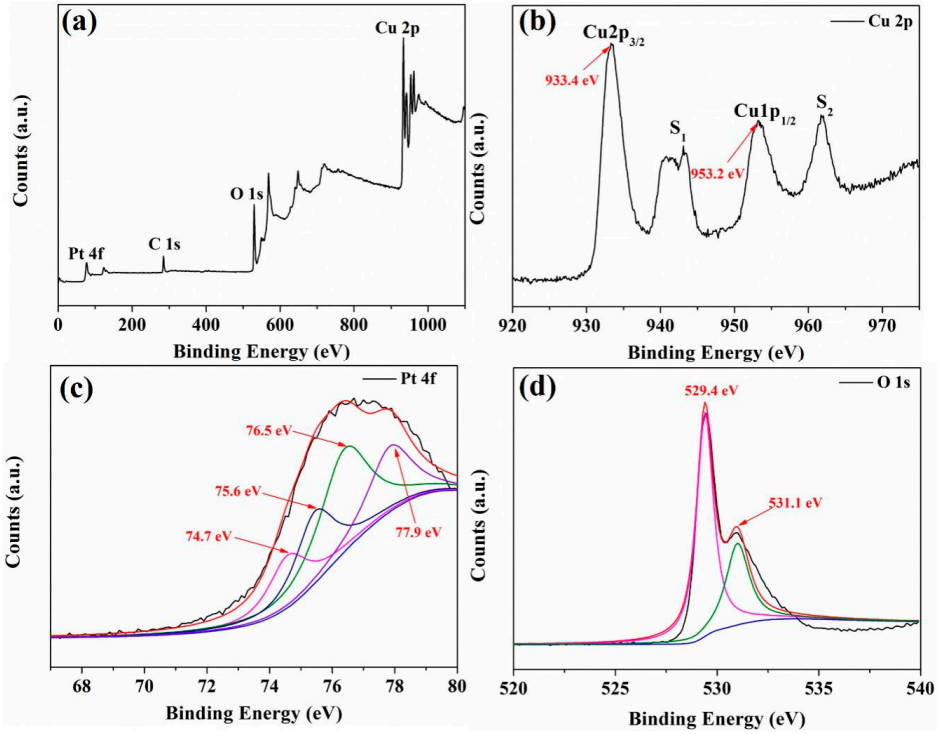

Figure 5. (**a**) X-ray photoelectron spectroscopy (XPS) spectrum of the 1.25 wt % Pt-doped CuO; (**b**–**d**) high-resolution spectra of Cu, Pt, and O peaks, respectively, (red line, blue line, purple line and green line are fitting curves).

The BET surface areas of the pure CuO and 1.25Pt-CuO were investigated via a BET method using N_2 adsorption and desorption. As shown in Figure 6, it has been shown that the BET surface area of the 1.25Pt-CuO is 24.3 m^2/g, which is 1.9 times larger than pure CuO (13.1 m^2/g). However, none of such two samples showed a porous structure based on the BET results. The larger surface area of the 1.25Pt-CuO can be beneficial for the enhancement of gas sensing properties.

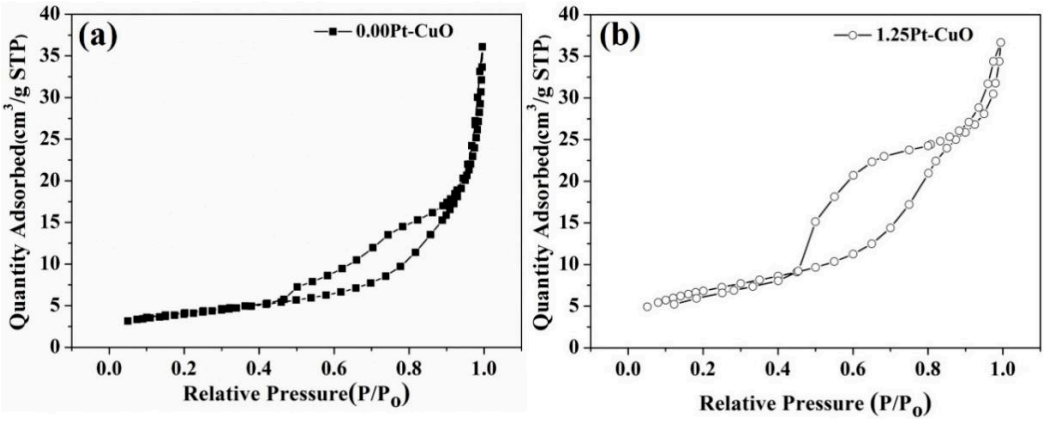

Figure 6. Typical N_2 adsorption-desorption isotherms of different specimens, as follows: (**a**) 0.00Pt-CuO and (**b**) 1.25Pt-CuO.

3.2. Gas Sensing Characteristics

To investigate the optimum operating temperature and additive amount of the Pt-doped CuO based sensor for H_2S, we examined the responses of the four sensors to 10 ppm H_2S gas from room temperature to 260 °C. Figure 7a illustrates that the response of all the doped sensors increased once the operating temperature changed from room temperatures to 40 °C, while the undoped sensor has its maximum response at 70 °C. Furthermore, all the Pt-doped sensors exhibit a much higher response than the pristine one. The 1.25Pt-CuO sensor showed the highest response of 135.1 to 10 ppm of H_2S gas at 40 °C, which was 13.1 times higher than that of the pure CuO sensor (R_g/R_a = 10.3) at the same temperature. At a high operating temperature (above 240 °C), the pure CuO and all Pt-doped sensors showed a small response (1.6–2.7). Therefore, the optimized doping concentration is 1.25 wt % Pt for CuO and the operating temperature is 40 °C. Figure 7b shows the dynamic response curves of the gas sensors, based on the pure CuO and Pt-doped CuO to 10 ppm H_2S at 40 °C. It proves that the 1.25Pt-CuO gas sensor has the highest response. However, it is noteworthy that neither the pure CuO sensor nor Pt-doped CuO sensor could be completely recovered to the baseline.

Figure 8 shows the sensing behavior of the sensor, based on 1.25 wt % Pt-doped CuO towards 10 ppm H_2S gas at 40 °C. As it is shown in Figure 8a, the resistance of the 1.25Pt-CuO sensor is 0.1 kΩ when exposed to air. After the sensor was exposed to H_2S gas, the response resistance increases to 13.51 kΩ, thus the response of the 1.25Pt-CuO sensor to 10 ppm H_2S is as high as 135.1 (R_g/R_a). Although the Pt-doped CuO sensors were highly sensitive to detect H_2S gas, the extremely long recovery time was the bottleneck for real practice. Figure 8b shows the dynamic response–recovery curves of the sensor; it took 37 s to reach 90% of the resistance variation. Figure 8b also shows that it took more than 3000 s to recover about 5% of the maximum value after removal of the H_2S. In fact, the response could not be completely recovered to the baseline, and it is the common issue for gas sensors operating at a low temperature. According to Chaturvedi et al. [37] because of molecular affinity, Cu and S could easily form a helical bond at a low operating temperature. Therefore, H_2S could be present in the form of molecular adsorption on the surface, and the adsorption is intermediate between physisorption and chemisorption.

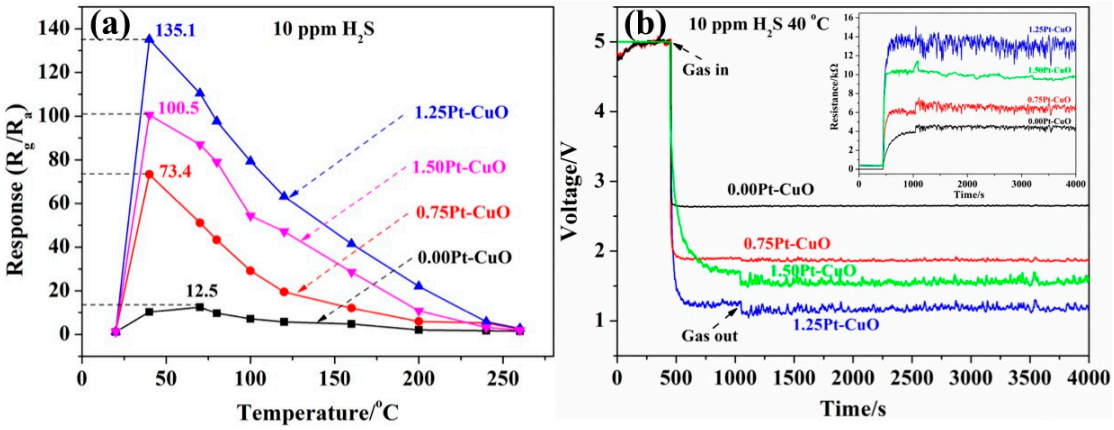

Figure 7. (**a**) Response of 0.00Pt-CuO, 0.75Pt-CuO, 1.25Pt-CuO, and 1.50Pt-CuO sensors to 10 ppm H_2S as a function of operating temperature; (**b**) the corresponding sensing transients of 0.00Pt-CuO, 0.75Pt-CuO, 1.25Pt-CuO, and 1.50Pt-CuO sensors to 10 ppm H_2S at 40 °C. The inset of (**b**) is the resistance variation of four sensors to 10 ppm H_2S at 40 °C.

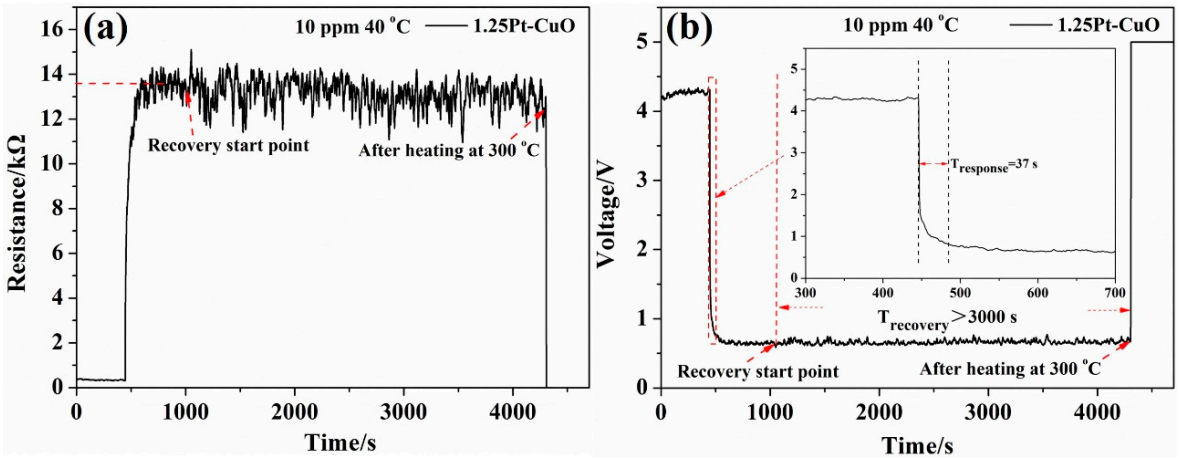

Figure 8. (**a**) The resistance variation of the 1.25Pt-CuO sensor to 10 ppm H_2S at 40 °C; (**b**) the corresponding sensing transients of the 1.25Pt-CuO sensor. The inset of (**b**) is the magnification of sensing transients between 300 s to 700 s.

In this work, we proposed a solution to solve the problem that the gas sensors could not be completely recovered at a low operating temperature. The principle of this scheme is based on the Joule heating effect, which accelerates the detachment of the H_2S molecules from the CuO surface by applying a short electric current pulse. As shown in Figure 9a, V_c is the test voltage; R_l is a load resistor, and the voltage drop on R_l is denoted as V_{out}; V_h is the heating voltage applied on the the heating wire; and V_m is the 4.6 V electric current pulse. Figure 9b shows the dynamic response curves of the 1.25Pt-CuO sensor to 1 ppm H_2S gas at 40 °C. Once the H_2S was removed and the sensor was exposed to air, the response could not be recovered to its original baseline. After applying a 4.6 V (the temperature was 300 °C) voltage pulse, the 1.25Pt-CuO sensor returned to its original state within 15 s. Reproducibility is an important indicator to evaluate the performance of the sensor. Figure 9b also shows the dynamic response curves of the 1.25Pt-CuO sensor to 10 ppm H_2S gas. In the five-cycle continuous test process, the sensors based on the Pt-doped CuO exhibit good stability, and their gas-sensing performance, such as sensitivity, and response/recovery speed did not show obvious resistance attenuation. In addition, such a 'recovery heating' process had tiny effect on the response of the sensor, which made the gas sensor highly reusable. Therefore, by applying a short electric current

pulse, we have developed high performance H_2S gas sensors based on the Pt-doped CuO with a low operating temperature.

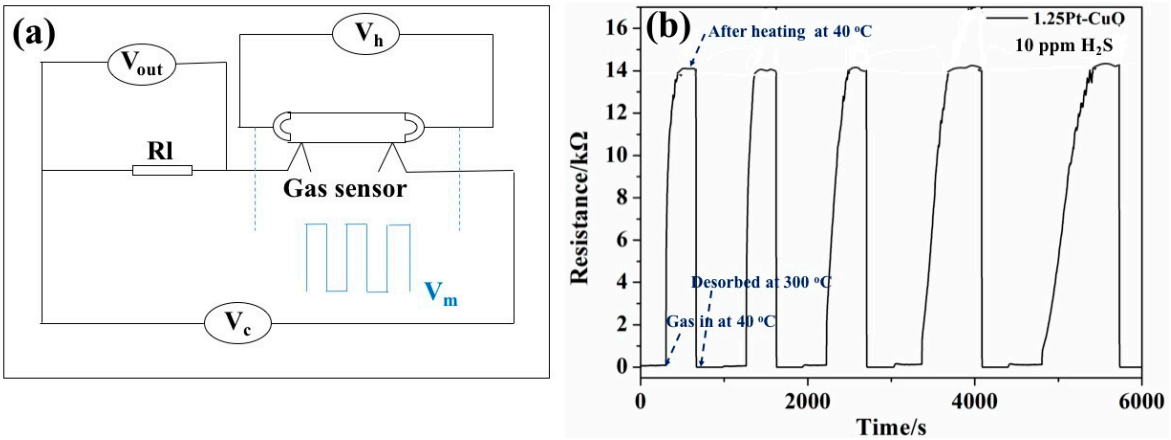

Figure 9. (**a**) Sensing diagram of the gas sensor with a 4.6 V electric modulation voltage; (**b**) the recovery cycles for 10 ppm H_2S of the 1.25Pt-CuO sensor at 40 °C, followed by a 4.6 V electric modulation voltage.

Selectivity is one of the key parameters of the gas sensors. To explore the selectivity of the sensors, the dynamic response curves of the 1.25Pt-CuO based sensor to 1 ppm H_2S and 50 ppm of other gases were measured at 40 °C. The results are shown in Figure 10a. Compared with the responses to H_2S gas, the responses to other reducing gases were negligible. Figure 10b shows the responses of the 1.25Pt-CuO sensor to various gas samples, including 50 ppm C_2H_5OH, NH_3, CH_3COCH_3, NO_2, Cl_2, H_2, NO, and 1 ppmH_2S, operated at 40 °C. The sensitivity of such sensors are 32.9 and 2.4 to 1 ppm H_2S and 50 ppm NO_2, respectively, while the responses to other gases ranged between 1.1 and 1.2. Therefore, 1.25 wt % Pt doping led to highest selectivity and sensitivity for the detection of H_2S at low operating temperature (i.e., 40 °C).

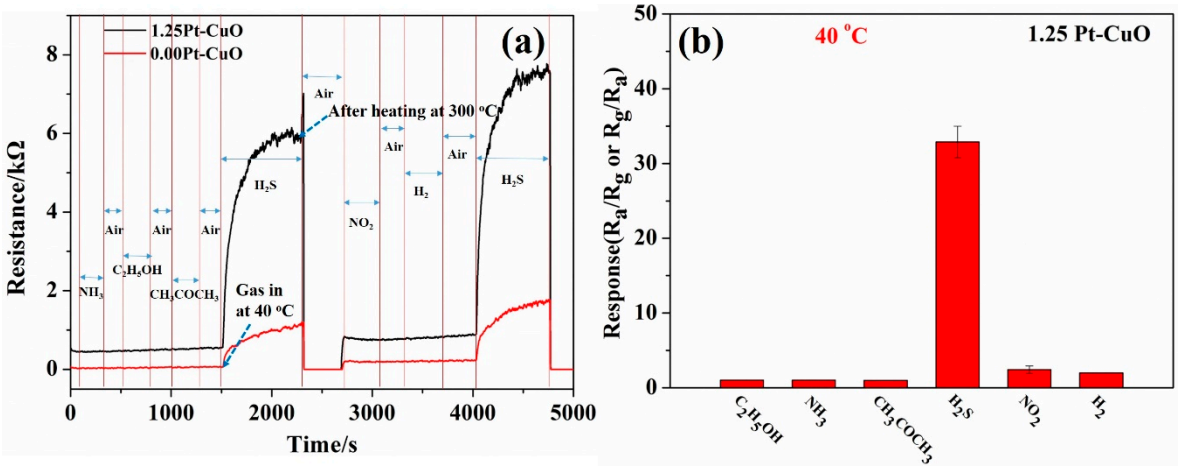

Figure 10. (**a**) Dynamic response curves of 1.25Pt-CuO and 0.00Pt-CuO based sensor to 1 ppm H_2S and 50 ppm various interfering gases at 40 °C; (**b**) gas response (R_a/R_g or R_g/R_a) of 1.25Pt-CuO to 50 ppm different gases and 1 ppm H_2S gas, operated at 40 °C.

Figure 11a displays the dynamic response–recovery transient of the sensor based on 1.25Pt-CuO, under the H_2S concentration ranging from 0.1 to 25 ppm, at the operating temperature of 40 °C. It is apparent that as the concentration of the H_2S gas increases, the response curve also displays a stepwise distribution. Figure 11b shows the response of the gas sensor to different concentrations of H_2S gas.

It can be observed that the gas response increased as the concentration increased. Even when the H_2S concentration is as low as 300 ppb, the response of the sensor is still 3.2. According to the value of response ($R_g/R_a > 2$), as the standard for a valid response [38], it can be said that the gas sensor based on 1.25Pt-CuO has a detection limit of H_2S gas as low as 300 ppb. Figure 12 illustrates the long-term stability of the gas sensor based on 1.25Pt-CuO. The results reveal that the response of the sensor changes by less than 10%, indicating that our sensor is stable and reliable.

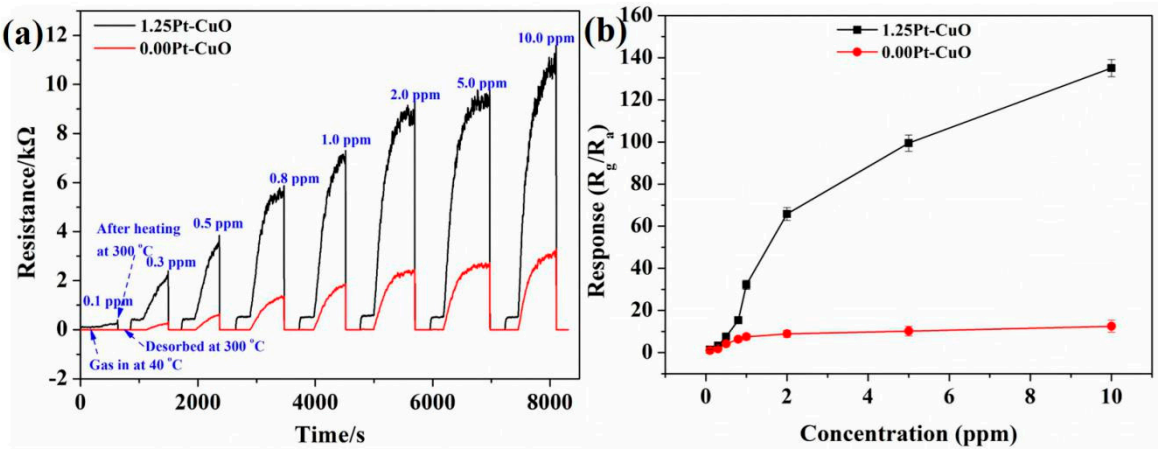

Figure 11. (**a**) Dynamic response transient of the gas sensor based on 1.25Pt-CuO and 1.00Pt-CuO to different concentrations of H_2S gas at 40 °C; (**b**) gas response of 1.25Pt-CuO and 1.00Pt-CuO sensor to different concentrations of H_2S at 40 °C.

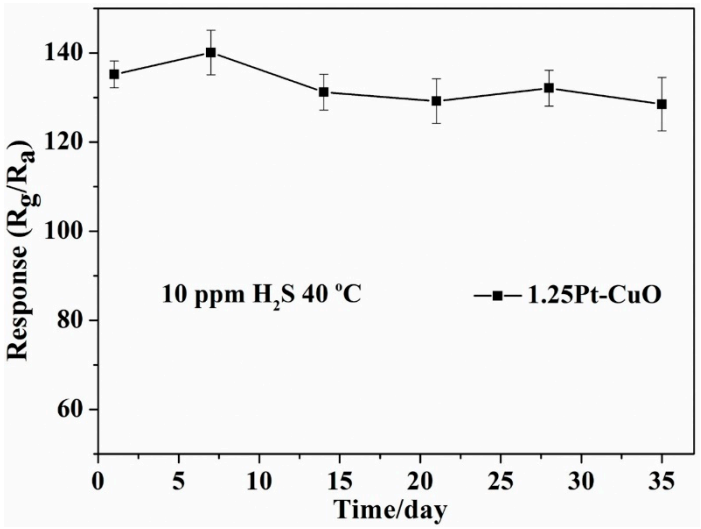

Figure 12. Long-term stability of 1.25Pt-CuO sensor to 10 ppm H_2S at 40 °C.

3.3. The Sensing Mechanism

The gas-sensing mechanism of the p-type semiconducting oxides has been previously reported, and it can be summarized as follows: Adsorption/desorption of gas molecules on the surface of semiconductors and reactions cause the change of resistance [11,24]. When the p-type CuO semiconductor is in contact with air, oxygen molecules are adsorbed on the surface of CuO and are ionized by electrons from the valence band, thereby generating negatively charged chemisorbed oxygen species (O^{2-}, O^-, and O_2^-), the processes are shown in Equations (1)–(4). The types of absorbed oxygen species depend on the operating temperature. Oxygen is absorbed on the surface as O_2^- ions below 147 °C or as O^- ions between 147–397 °C. Above 397 °C, O^{2-} ions occur [39].

According to the above conclusions, the major oxygen adsorption species on the surface of CuO is O_2^- when the operating temperature is 40 °C.

$$O_2\ (gas) \rightarrow O_2\ (ads) \quad (1)$$

$$O_2\ (ads) + e^- \rightarrow O_2^-\ (ads)\ (<147\ ^\circ C) \quad (2)$$

$$O_2^-\ (ads) + e^- \rightarrow 2O^-\ (ads)\ (147\ ^\circ C\text{-}397\ ^\circ C) \quad (3)$$

$$O^-\ (ads) + e^- \rightarrow O^{2-}\ (ads)\ (>397\ ^\circ C) \quad (4)$$

Once the sensor is exposed to an H_2S (reducing gas) atmosphere operating at 40 °C, the H_2S molecules are oxidized by O_{2-} to form SO_2 and H_2O, while releasing electrons [40], and the sensing reaction is as shown in Equation (5).

$$H_2S\ (g) + 3O_2^-\ (ads) \rightarrow H_2O\ (g) + SO_2\ (g) + 6e^- \quad (5)$$

The released electrons during this process will recombine with the holes on the surface of CuO and cause the decrease of hole concentration, which will lead to an increased resistance of the gas sensor. According to some previous reports [41,42], a CuS layer might form on the surface of the CuO, when the sensor is exposed to high H_2S concentrations, the spontaneous chemical reaction is as shown in Equation (6), as follows:

$$CuO\ (s) + H_2S\ (g) \rightarrow CuS\ (s) + H_2O\ (g) \quad (6)$$

In order to confirm the formation of CuS, we have carried out XPS studies on a 10 ppm H_2S exposed 1.25Pt-CuO sensor. The recorded Cu 2p and S 2p spectra are shown in Figure 13. When the sensor was exposed to H_2S gas, the Cu 2p spectrum confirmed the presence of CuO and CuS, and the corresponding peak of 169.2 eV in the S 2p spectrum also confirmed the presence of CuS [11].

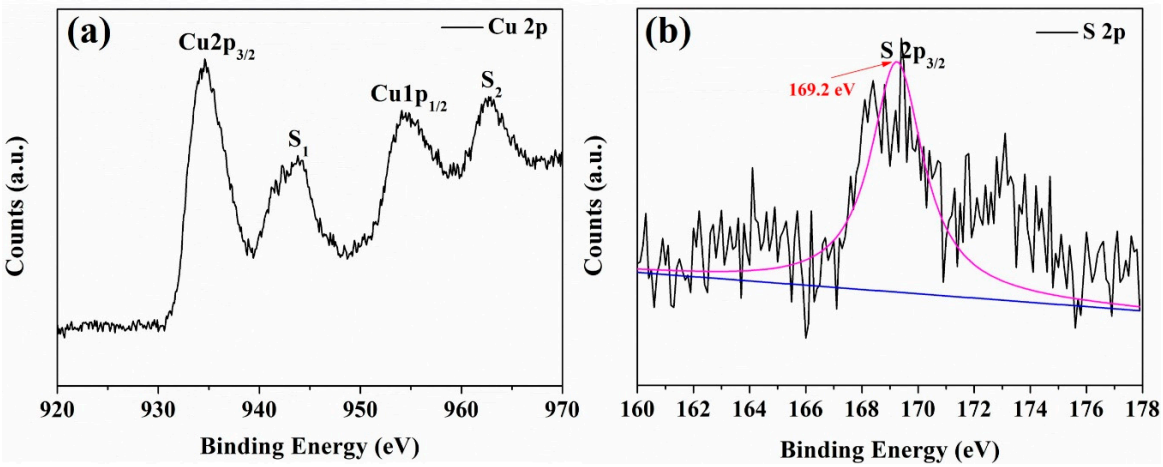

Figure 13. (**a**) Cu 2p and (**b**) S 2p XPS spectra recorded for 1.25 wt % Pt-doped CuO after exposure to 10 ppm H_2S.

Once H_2S is removed by introducing air, the CuS is unstable, and is able to be slowly oxidized by oxygen in the air, as shown in Equation (7). As a result, recovery of the resistance will occur.

$$CuS\ (s) + O_2\ (g) \rightarrow 2CuO\ (s) + 2S\ (s) \quad (7)$$

The influence of Pt dopant on the gas sensing properties of the sensor can be attributed to the spillover effect [43]. Various chemisorbed oxygen species and gas molecules were able to spill over

onto the surface CuO support, as the O_2 and H_2S gas molecules are absorbed in the abundant sites provided by the Pt dopant. Thus, it is reasonable to believe that the better gas sensing properties of the Pt-doped CuO is mainly caused by the ability of the Pt dopant to accelerate the electron exchange between the test gas and the sensor, rather than being directly involved in the reaction. On the other hand, compared with pure CuO, 1.25Pt-doped CuO nanoflowers have a larger BET surface area, which can provide more adsorption sites for gas adsorption. However, as the doping concentration increased to 1.50 wt %, a constipation disorder occurs and the surface density increases, resulting in Fermi level changes and the decrease of sensor response [44]. In summary, the doping of Pt is the main reason for the enhanced performance of CuO-based sensors.

4. Conclusions

H_2S sensors based on Pt-doped CuO nano-flowers were developed. The pristine and Pt-doped CuO nano-flowers were fabricated by a simple heating route using a water bath, and their gas-sensing performances toward H_2S were thoroughly investigated. The Pt-doped CuO sensor exhibited a significant improvement in its H_2S performance compared with the sensors based on pristine CuO. The enhanced sensing performances of Pt doped CuO would be most likely ascribed to the spillover effect. At an operating temperature of 40 °C, the optimized Pt-doped CuO sensor yielded a response of 135.1 and 32.9 upon exposure to H_2S gas of 10 and 1 ppm, respectively. To solve the issue of a long recovery time at a low operating temperature, a 4.6 V (300 °C) heater voltage pulse was selected, and the recovery time could be shortened to 15 s.

Author Contributions: Q.T. and X.-B.H. carried out the experiment and draft the manuscript, M.H. and L.-L.X. carried out gas sensor test, Z.-G.Z. and J.-Q.W. are the corresponding author for the whole work.

Funding: This work was supported by the National Natural Science Foundation of China (No. 61471233), the Program for Professor of Special Appointment (Eastern Scholar) at SIHL, Shuguang Project by Shanghai Municipal Education Commission (No. 14SG52).

Conflicts of Interest: The authors declare no conflict of interest.

References

1. Hendrickson, R.G.; Chang, A.; Hamilton, R. Co-worker fatalities from hydrogen sulfide. *Am. J. Ind. Med.* **2004**, *45*, 346–350. [CrossRef] [PubMed]
2. Guo, Y.N.; Gong, M.M.; Li, Y.S.; Liu, Y.L.; Dou, X.C. Sensitive, selective, and fast detection of ppb-level H_2S gas boosted by ZnO-CuO mesocrystal. *Nanoscale Res. Lett.* **2016**, *475*, 1–9. [CrossRef] [PubMed]
3. Hu, X.B.; Zhu, Z.G.; Chen, C.; Wen, T.Y.; Zhao, X.L.; Xie, L.L. Highly sensitive H_2S gas sensors based on Pd-doped CuO nanoflowers with low operating temperature. *Sens. Actuators B Chem.* **2017**, *253*, 809–817. [CrossRef]
4. Nagarajan, V.; Chandiramouli, R. DFT studies on interaction of H_2S gas with α-Fe_2O_3 nanostructures. *J. Inorg. Organomet. Polym. Mater.* **2016**, *26*, 394–404. [CrossRef]
5. Li, W.H.; Sun, W.; Xu, X.Q.; Du, L.P.; Li, M.Y. Coumarin-based fluorescent probes for H_2S detection. *J. Fluoresc.* **2013**, *23*, 181–186. [CrossRef] [PubMed]
6. Zhang, Y.Y.; Zhang, H.; Wu, P.; Zhang, H.R.; Xu, J.J.; Chen, H.Y. In situ activation of CdS electrochemiluminescene film and its application in H_2S detection. *Anal. Chem.* **2014**, *86*, 8657–8664. [CrossRef] [PubMed]
7. Henthorn, H.A.; Pluth, M.D. Mechanistic insights into the H_2S-mediated reduction of aryl azides commonly used in H_2S detection. *J. Am. Chem. Soc.* **2015**, *135*, 15330–15336. [CrossRef] [PubMed]
8. Franke, M.E.; Koplin, T.J.; Simon, U. Metal and metal oxide nanoparticles in chemiresistors: Does the nanoscale matter? *Small* **2006**, *2*, 36–50. [CrossRef] [PubMed]
9. Tricoli, A.; Righettoni, M.; Teleki, A. Semiconductor gas sensors: Dry synthesis and application. *Angew. Chem. Int. Ed.* **2010**, *49*, 7632–7659. [CrossRef] [PubMed]

10. Oosthuizen, D.N.; Motaung, D.E.; Swart, H.C. In depth study on the notable room-temperature NO_2 gas sensor based on CuO nanoplatelets prepared by sonochemical method: Comparison of various bases. *Sens. Actuators B Chem.* **2018**, *266*, 761–772. [CrossRef]
11. Ramgir, N.S.; Ganapathi, S.K.; Kaur, M.; Datta, N.; Muthe, K.P.; Aswal, D.K.; Gupta, S.K.; Yakhmi, J.V. Sub-ppm H_2S sensing at room temperature using CuO thin films. *Sens. Actuators B Chem.* **2010**, *151*, 90–96. [CrossRef]
12. Xu, J.Q.; Wang, X.H.; Shen, J.N. Hydrothermal synthesis of In_2O_3 for detecting H_2S in air. *Sens. Actuators B Chem.* **2006**, *115*, 642–646. [CrossRef]
13. Wang, C.H.; Chu, X.F.; Wu, M.M. Detection of H_2S down to ppb levels at room temperature using sensors based on ZnO nanorods. *Sens. Actuators B Chem.* **2006**, *113*, 320–323. [CrossRef]
14. Song, Z.L.; Wei, Z.; Wang, B.C.; Luo, Z.; Xu, S.M.; Zhang, W.K.; Yu, H.X.; Li, M.; Huang, Z.; Zang, J.F.; et al. Sensitive room-temperature H_2S gas sensors employing SnO_2 quantum wire/reduced graphene oxide nanocomposites. *Chem. Mater.* **2016**, *28*, 1205–1212. [CrossRef]
15. Zhang, Y.; Xiang, Q.; Xu, J.Q.; Xu, P.C.; Pan, Q.Y.; Li, F. Self-assemblies of Pd nanoparticles on the surface of single crystal ZnO nanowires for chemical sensors with enhanced performances. *J. Mater. Chem.* **2009**, *27*, 4701–4706. [CrossRef]
16. Tao, W.H.; Tsai, C.H. H_2S sensing properties of noble metal doped WO_3 thin film sensor fabricated by micromachining. *Sens. Actuators B Chem.* **2002**, *81*, 237–247. [CrossRef]
17. Demel, J.; Zhigunov, A.; Jirka, I.; Klementova, M.; Lang, K. Facile synthesis of CuO nanosheets via the controlled delamination of layered copper hydroxide acetate. *J. Colloid Interface Sci.* **2015**, *452*, 174–179. [CrossRef] [PubMed]
18. Mai, Y.J.; Wang, X.L.; Xiang, J.Y.; Qiao, Y.Q.; Zhang, D.; Gu, J.P.; Tu, J.P. CuO/graphene composite as anode materials for lithium-ion batteries. *Electrochim. Acta* **2011**, *56*, 2306–2311. [CrossRef]
19. Wang, G.L.; Huang, J.C.; Chen, S.L.; Gao, Y.Y.; Cao, D.X. Preparation and supercapacitance of CuO nanosheet arrays grown on nickel foam. *J. Power Sources* **2011**, *196*, 5756–5760. [CrossRef]
20. Nezamzadeh, E.A.; Hushmandrad, S. Solar photodecolorization of methylene blue by CuO/X zeolite as a heterogeneous catalyst. *Appl. Catal. A Gen.* **2010**, *388*, 149–159. [CrossRef]
21. Capone, S.; Forleo, A.; Francioso, L.; Rella, R.; Siciliano, P.; Spadavecchia, J.; Presicce, D.S.; Taurino, A.M. Solid state gas sensors: State of the art and future activities. *J. Optoelectron. Adv. Mater.* **2003**, *5*, 1335–1348. [CrossRef]
22. Kim, K.M.; Jeong, H.M.; Kim, H.R.; Choi, K.I.; Kim, H.J.; Lee, J.H. Selective detection of NO_2 using Cr-doped CuO nanorods. *Sensors* **2012**, *12*, 8013–8025. [CrossRef] [PubMed]
23. Kim, H.; Jin, C.; Park, S.; Kim, S.; Lee, C.M. H_2S gas sensing properties of bare and Pd-functionalized CuO nanorods. *Sens. Actuators B Chem.* **2012**, *161*, 594–599. [CrossRef]
24. Liu, S.; Yu, B.; Zhang, H.; Fei, T.; Zhang, T. Enhancing NO_2 gas sensing performances at room temperature based on reduced graphene oxide-ZnO nanoparticles hybrids. *Sens. Actuators B Chem.* **2014**, *202*, 272–278. [CrossRef]
25. Ivanov, P.; Llobet, E.; Vilanova, X.; Brezmes, J.; Hubalek, J.; Correig, X. Development of high sensitivity ethanol gas sensors based on Pt-doped SnO_2 surface. *Sens. Actuators B Chem.* **2004**, *99*, 201–206. [CrossRef]
26. Wang, Y.; Wang, S.R.; Zhao, Y.Q.; Zhu, B.L.; Kong, F.H.; Wang, D.; Wu, S.H. H_2S sensing characteristics of Pt-doped α-Fe_2O_3 thick film sensors. *Sens. Actuators B Chem.* **2007**, *125*, 79–84. [CrossRef]
27. Miller, D.; Akbar, S.; Morris, P. Nanoscale metal oxide-based heterojunctions for gas sensing: A review. *Sens. Actuators B Chem.* **2014**, *204*, 250–272. [CrossRef]
28. Kayestha, R.; Sumati; Hajela, K. ESR studies on the effect of ionic radii on displacement of Mn^{2+} bound to a soluble β-galactoside binding hepatic lectin. *FEBS Lett.* **1995**, *368*, 285–288. [CrossRef]
29. Sheppard, L.R.; Lamo, M.B.; Holik, J.; Mayfield, K.J.; Nelson, D.R. Solute diffusion of platinum in rutile titanium dioxide. *J. Am. Ceram. Soc.* **2013**, *96*, 407–411. [CrossRef]
30. Wang, D.G.; Wang, Y.Q.; Jiang, T.T.; Jia, H.X.; Yu, M.H. The preparation of M (M: Mn^{2+}, Cd^{2+}, Zn^{2+})-doped CuO nanostructures via the hydrothermal method and their properties. *J. Mater. Sci. Mater. Electron.* **2016**, *27*, 2138–2145. [CrossRef]
31. Petr, V.; Václav, Š.; Jirˇí, H.; Martin, K. Shape-controlled synthesis of Sn-doped CuO nanoparticles for catalytic degradation of Rhodamine B. *J. Colloid Interface Sci.* **2016**, *481*, 28–38.

32. Zhang, Y.W.; Si, R.; Liao, C.S.; Yan, C.H. Facile alcohothermal synthesis, size-dependent ultraviolet absorption, and enhanced CO conversion activity of ceria nanocrystals. *J. Phys. Chem. B* **2003**, *107*, 10159–10167. [CrossRef]
33. Hu, X.B.; Zhu, Z.G.; Li, Z.H.; Xie, L.L.; Wu, Y.H.; Zheng, L.Y. Heterostructure of CuO microspheres modified with $CuFe_2O_4$ nanoparticles for highly sensitive H_2S gas sensor. *Sens. Actuators B Chem.* **2018**, *264*, 139–149. [CrossRef]
34. Liu, L.Q.; Zhou, F.; Wang, L.G.; Qi, X.J.; Shi, F.; Deng, Y.Q. Low-temperature CO oxidation over supported Pt, Pd catalysts: Particular role of FeO_x support for oxygen supply during reactions. *J. Catal.* **2010**, *274*, 1–10. [CrossRef]
35. Wang, S.R.; Zhang, J.X.; Yang, J.D.; Gao, X.L.; Zhang, H.X.; Wang, Y.S.; Zhu, Z.Y. Spinel $ZnFe_2O_4$ nanoparticle-decorated rod-like ZnO nanoheterostructures for enhanced gas sensing performances. *RSC Adv.* **2015**, *5*, 10048–10057. [CrossRef]
36. Hu, D.; Han, B.Q.; Deng, S.J.; Feng, Z.P.; Wang, Y.; Popovic, J.; Nuskol, M.; Wang, Y.; Djerdj, I. Novel mixed phase SnO_2 nanorods assembled with SnO_2 nanocrystals for enhancing gas-sensing performance toward isopropanol gas. *J. Phys. Chem. C* **2014**, *118*, 9832–9840. [CrossRef]
37. Chaturvedi, S.; Rodriguez, J.A.; Hrbek, J. Reaction of S_2 with ZnO and Cu/ZnO surfaces: Photoemission and molecular orbital studies. *J. Phys. Chem. B* **1997**, *101*, 10860–10869. [CrossRef]
38. Cho, Y.H.; Liang, X.; Kang, Y.C.; Lee, J.H. Ultrasensitive detection of trimethylamine using Rh-doped SnO_2 hollow spheres prepared by ultrasonic spray pyrolysis. *Sens. Actuators B Chem.* **2015**, *207*, 330–337. [CrossRef]
39. Sun, Y.F.; Liu, S.B.; Meng, F.L.; Liu, J.Y.; Jin, Z.; Kong, L.T.; Liu, J.H. Metal oxide nanostructures and their gas sensing properties: A Review. *Sensors* **2012**, *1*, 36–50. [CrossRef] [PubMed]
40. Liu, X.H.; Zhang, J.; Kang, Y.F.; Wu, S.H.; Wang, S.R. Brochantite tabular microspindles and their conversion to wormlike CuO structures for gas sensing. *CrystEngComm* **2012**, *14*, 620–625. [CrossRef]
41. Park, S.; Kim, S.; Kheel, H.; Hyun, S.K.; Jin, C.; Lee, C. Enhanced H_2S gas sensing perfoemane of networked CuO-ZnO composite nanoparticle sensor. *Mater. Res. Bull.* **2016**, *82*, 130–135. [CrossRef]
42. Sonia, S.; Kumar, P.S.; Jayram, N.D.; Masuda, Y.; Manqalaraj, D.; Lee, C. Superhydrophobic and H_2S gas sensing properties of CuO nanostructured thin films through a successive ionic layered adsorption reaction process. *RSC Adv.* **2016**, *6*, 24290–24298. [CrossRef]
43. Kappler, J.; Barsan, N.; Weimar, U.; Dieguez, A.; Alay, J.L.; Rodriguez, A.R.; Morante, J.R.; Gopel, W. Correlation between XPS, Raman and TEM measurements and the gas sensitivity of Pt and Pd doped SnO_2 based gas sensors. *Fresenius' J. Anal. Chem.* **1998**, *361*, 110–114. [CrossRef]
44. Korotcenkov, G.; Boris, I.; Brinzari, V.; Han, S.H.; Cho, B.K. The role of doping effect on the response of SnO_2-based thin film gas sensors: Analysis based on the results obtained for Co-doped SnO_2 films deposited by spray pyrolysis. *Sens. Actuators B Chem.* **2013**, *182*, 112–124. [CrossRef]